DOI: 10.2352/ISSN.2470-1173.2016.19.COIMG-173
Reprinted from
Journal of Imaging Science and Technology® 59(6): 060406-1–060406-11, 2015.

Exploiting Structure and Variable Dependency Modeling in Block-based Compressed Sensing Image Reconstruction in the Presence of Non-linear Mixtures

Lynn M. Keuthan and Robert J. Harrington
Electrical and Computer Engineering, The George Washington University, Washington, DC 20052, USA
E-mail: keuthan@gwu.edu

Jefferson M. Willey
Naval Research Laboratory, Washington, DC 20375, USA

Abstract. *With the introduction of compressed sensing (CS) theory, investigation into exploiting sparseness and optimizing compressive sensing performance has ensued. Compressed sensing is highly applicable to images, which naturally have sparse representations. Improvements in the area of image denoising have resulted from the combination of highly-directional transforms with shrinkage and thresholding techniques along with imposition of a model to account for statistical properties of images. Using this approach, statistical modeling of dependencies in the transform domain is incorporated into high-performance and efficient state-of-the-art CS image reconstruction algorithms with highly-directional transforms incorporating redundancy and bivariate shrinkage and thresholding to further refine image reconstruction performance improvements. Additionally, hierarchical structural dependency modeling is incorporated to account for parent–child coefficient relationships. These techniques exploit hierarchical structure and multiscale subbands of frequencies and orientation, exploiting dependencies across and within scales. Additionally, these techniques are incorporated with minimal additional CPU execution time into block-based CS (BCS) algorithms, which are known for their efficient and fast computation time. Experimental results show increased refinements of image reconstruction performance over current state-of-the-art image reconstruction algorithms, particularly at the higher CS ratios (lower sampling rates) of interest in compressed sensing.* © *2015 Society for Imaging Science and Technology.*
[DOI: 10.2352/J.ImagingSci.Technol.2015.59.6.060406]

INTRODUCTION

Compressed sensing (CS) theory shows that it is possible to defy the Nyquist Sampling Theorem and still recover complete signal information in signals with sparse representations in some transform domain.[1,2] The Nyquist Sampling Theorem presents required minimum sampling limits based on signal band limitedness. However, compressed sensing shows that data and signals in many real-world problems (composed of sparse non-linear mixtures) can be accurately represented by sparse representations. Indeed, application of compressed sensing in imaging, video, and audio applications has been advantageous due to the fact that most images and video and audio recordings of practical interest have sparse representations in a transform domain.

Given the ability to recover information from a non-linear mixture, compressed/sparse sensing is a promising area to explore the addressing of optimization of signal reconstruction based on accounting for variable dependencies in a non-linear signal. Initial compressed sensing recovery techniques assumed that the sparsity transform coefficients were independently distributed, and these techniques did not exploit dependencies between transform coefficients to improve recovery performance. More recently, some algorithms have been proposed to exploit some variable dependencies for improved compressed sensing recovery. To efficiently exploit variable dependencies, the nature and characteristics of the dependencies need to be accurately accounted for. This article proposes to apply theoretical properties of highly-directional and redundant transforms, and the optimized structural and statistical modeling of dependencies, in the reconstruction algorithm to improve image reconstruction and feature optimization in the presence of non-linear mixtures.

Hierarchical structure in the transform domain of the Discrete Wavelet Transform (DWT), Dual-tree Discrete Wavelet Transform (DDWT) and Contourlet Transform (CT) is exploited by incorporating modeling of dependencies between parent and associated child coefficients using statistical properties shown to accurately model variable dependencies in images. These statistical properties are also used to model dependencies within intra-scale neighborhoods of transform domain coefficients for the DWT, DDWT, Discrete Cosine Transform (DCT) and CT Block-based Compressed Sensing (BCS) Smoothed Projected Landweber (SPL) algorithms. Although some previous algorithms have applied statistical modeling in the transform domain to improve image reconstruction performance, as discussed in our previous published research,[3] the proposed combination of structural and statistical modeling with application of highly-directional transforms and thresholding and shrinkage techniques shows that the combined application of these techniques provides improved image reconstruction results.

Received June 30, 2015; accepted for publication Oct. 12, 2015; published online Dec. 15, 2015. Associate Editor: Chunghui Kuo.
1062-3701/2015/59(6)/060406/11/$25.00

DOI: 10.2352/ISSN.2470-1173.2016.19.COIMG-173

BACKGROUND

The goal of compressed sensing is to find sparse solutions given compressive linear measurements. For example, undersampled linear measurements $\mathbf{b} \in \mathbb{R}^M$ obtained by an undersampled imaging system can be expressed as

$$\mathbf{b} = \mathbf{\Phi}\mathbf{\Psi}^{-1}\mathbf{x}, \tag{1}$$

where

$$\mathbf{x} = \mathbf{\Psi}\mathbf{y} \in \mathbb{R}^N \tag{2}$$

denotes sparse transform coefficients of the vector image $\mathbf{y} \in \mathbb{R}^N$ and the CS matrix is composed of an $M \times N$ compressive measurement matrix $\mathbf{\Phi}$ and the inverse of a sparsity transform $\mathbf{\Psi}^{-1}$ (such as DWT or Discrete-Cosine Transform), where $M \ll N$.[1,2,4,5]

A fundamental criterion for compressed sensing performance is sparsity of signals in the transform domain. For an S-sparse signal, coefficients are represented as S non-zero entries (with the remaining entries set to zero). An S-compressible signal is sufficiently approximated by the S largest coefficients. Exact signal recovery can be achieved if an N-dimensional signal is S-sparse and if the number of incoherent linear measurements follows

$$M \geq O(S\log(N/S)). \tag{3}$$

An additional condition for compressed sensing is the Restricted Isometry Property (RIP), which is an incoherence condition for the sensing matrix used to acquire the measurements.[6] This guarantees an approximately orthonormal projection for any S-sparse signal. Given signal sparsity and the RIP, signals can be reconstructed from noisy measurements by solving the l_1 minimization problem:

$$\arg\min_x \|\mathbf{x}\|_1 \quad \text{such that } \|\mathbf{b} - \mathbf{\Phi}\mathbf{\Psi}^{-1}\mathbf{x}\|_2^2 \leq \varepsilon,$$

where the $l_\mathbf{P}$ norm is defined as

$$\|\mathbf{x}\|_P = \left(\sum_i |\mathbf{x}(i)|^P\right)^{1/P}. \tag{4}$$

By solving the l_1 minimization problem, it becomes a constrained optimization problem. A penalty function is utilized with a Lagrangian multiplier λ:

$$\|\mathbf{b} - \mathbf{\Phi}\mathbf{\Psi}^{-1}\mathbf{x}\|_2^2 + \lambda\|\mathbf{x}\|_1, \tag{5}$$

where the regularization parameter λ modulates the relative importance between data consistency and the l_1 norm penalty.

The CS reconstruction problem is the regularization of the inverse problem:

$$\mathbf{y} = \mathbf{\Psi}^{-1}\mathbf{x}. \tag{6}$$

Energy compact representations provided by transforms typically yield compressible representations of signals, which allows application of CS Theory to a diverse set of signals.

Compressed sensing reconstruction algorithms are usually iterative. They use the previous signal estimate in consequent reconstruction to identify significant coefficients. They implicitly or explicitly introduce weights, which are often based on the magnitude of the former signal estimate. Early CS reconstruction algorithms typically do not exploit nor account for signal dependencies between coefficients. They typically set:

$$w^k(i) = 1/|x^{k-1}(i)|, \tag{7}$$

where $w^k(i)$ denotes a weight associated with the wavelet coefficient $x^k(i)$ and $x^{k-1}(i)$ denotes the wavelet coefficient at iteration $k-1$.

The Iterative Hard-Thresholding (IHT) compressed sensing reconstruction algorithms, of interest herein, solve the S-sparse problem[7,8]

$$\arg\min_x \|\mathbf{b} - \mathbf{\Phi}\mathbf{\Psi}^{-1}\mathbf{x}\|_2^2 \quad \text{such that } \|\mathbf{x}\|_0 \leq S, \tag{8}$$

using the iterative algorithm

$$\begin{aligned} \ddot{\mathbf{x}}^k &= \dot{\mathbf{x}}^k + (1/\gamma)\mathbf{\Psi}\mathbf{\Phi}^T(\mathbf{b} - \mathbf{\Phi}\mathbf{\Psi}^{-1}\dot{\mathbf{x}}^k) \\ \dot{\mathbf{x}}^{k+1} &= \begin{cases} \ddot{\mathbf{x}}^k, & |\ddot{\mathbf{x}}^k| \geq \tau^{(k)}; \\ 0, & \text{otherwise}, \end{cases} \end{aligned} \tag{9}$$

where γ is a scaling factor and $\tau^{(k)}$ is a threshold set appropriately at each iteration. Haupt and Nowak in Ref. 9 use the largest eigenvalue of $\mathbf{\Phi}^T\mathbf{\Phi}$ to set the scaling factor γ. Techniques based on projections form $\dot{\mathbf{x}}$ by successively projecting and thresholding. It is noted that Projected Landweber (PL) algorithms of the IHT class provide reduced computational complexity.

Lu and Do,[10] Blumensath and Davies,[11] and Baraniuk et al.[12] have shown theoretically that it is possible to substantially decrease the number of measurements needed for robust recovery in CS by incorporating more realistic signal models into signal recovery. More recently, some algorithms have incorporated structural dependency models into algorithms, and these have, indeed, yielded improved image reconstruction. For single image reconstruction (for modeling dependencies within the single image, which can vary highly in regard to correlation between 'neighbors'), the BCS-SPL-DWT, BCS-SPL-DDWT, BCS-SPL-DCT and BCS-SPL-CT algorithms,[13] particularly the BCS-SPL-DDWT, BCS-SPL-DCT and BCS-SPL-CT versions, appear to outperform many other proposed CS image reconstruction algorithms.[3] In addition, the BCS-SPL algorithms as a whole, being block-based, tend to execute ~1.5 to 110 times faster than other algorithms based on published CPU execution times.[3,13] Therefore, the enhanced algorithmic modification proposed herein was applied to these four state-of-the-art algorithms.

Additional considerations for optimizing CS reconstruction can be gained from related research in image denoising. In image denoising, one successful technique has been to apply spatially adaptive wavelet thresholding with context modeling.[14] In addition, significant improvement comes from the use of representations with a higher degree of redundancy, as well as increased selectivity in

DOI: 10.2352/ISSN.2470-1173.2016.19.COIMG-173

orientation.[15–18] It is also noted that denoising solutions (such as estimating local signal variance and then applying the standard linear least squares (LLS) solution) can be substantially more powerful when applied in a multiscale oriented representation.[15,19–23] Also, solutions based on Gaussian-scale Mixtures (GM) models, with different prior assumptions about the hidden variables, have produced some of the most effective methods for removing homogeneous additive noise from natural images to date.[24]

This article proposes to explore further optimization of reconstruction algorithms by applying these theoretical principles, and the structural and statistical modeling of dependencies, in the reconstruction algorithm to improve image reconstruction and feature optimization in the presence of non-linear mixtures.

TECHNICAL APPROACH

In the wavelet transform domain of natural images, the amplitudes of coefficients in similar positions, orientations, and scales are highly correlated. These higher-order dependencies, as well as the higher-order marginal statistics, may be modeled as Gaussian distributions with a hidden Markov model (hidden random variable). This can be characterized by Gaussian-scale Mixtures, which can account for both marginal and pairwise joint distributions of wavelet coefficients.[25,26] Gaussian-scale Mixtures (GM) densities are symmetric and zero-mean, and they have leptokurtotic marginal densities (i.e., heavier tails than a Gaussian). They represent an important subset of the elliptically symmetric distribution, which are those that can be defined as functions of a quadratic equation norm of the random vector.

Our approach to optimization is to incorporate optimized structural and statistical image dependency characteristics into the compressed sensing reconstruction algorithms to optimize reconstruction performance. This will account for variable dependencies and optimize performance of compressed sensing for many real-world applications, including image processing, particularly in regard to reconstruction of natural images with random-appearing/complex dependencies.

We focus on highly-directional sparsifying transforms, an overcomplete tight frame representation, and the Bayes Least Squares-Gaussian-scale Mixtures (BLS-GM) model and hierarchical structural dependency modeling to model dependencies and optimize reconstruction of images. Sparsifying transforms, such as the Discrete Wavelet Transform (DWT), the Dual-tree DWT (DDWT), the Discrete Cosine Transform (DCT), and the Contourlet Transform (CT), are used for spatial dependencies such as in natural images and provide multiresolution and local characteristics of the signal. Highly-directional transforms such as the DDWT and CT are utilized, which have significant directional selectivity and redundancy, with the DDWT, taken as a whole, being a redundant tight frame. This can exploit hierarchical structure and multiscale subbands of frequency and orientation, exploiting dependencies across and within scales. Bayes Least Squares-Gaussian-scale Mixtures (BLS-GM) accurately describe statistical dependencies of wavelet coefficients in images,[24] and, therefore, can be incorporated to further address dependencies and optimize performance. Furthermore, hierarchical structural dependencies between parent- and child-coefficients as well as neighborhood coefficients in the transform domain are incorporated within the model.

As discussed, one of the best-performing state-of-the-art algorithms is the Block-based Compressed Sensing Smoothed Projected Landweber (BCS-SPL),[13] which employs smoothing and the bivariate shrinkage method. The BCS-SPL-DDWT and BCS-SPL-CT also employ highly-directional and redundant transforms.

We utilize a Bayes Least Squares-Gaussian-scale Mixtures (BLS-GM) model and hierarchical structural dependency modeling within the BCS-SPL-DWT, BCS-SPL-DDWT, BCS-SPL-DCT and BCS-SPL-CT algorithms to model the statistical dependencies of wavelet coefficients in the sparsity domain. This enhanced modeling of the wavelet coefficients further accounts for the dependencies between neighboring coefficients and enhances the detection of features and image reconstruction. In particular, more significant coefficients are given additional weight, thereby emphasizing and enhancing features and boundary/edge detection.

We incorporate this model into algorithms through the iterative application of weights in the transform domain by (1) computing an intermediate signal estimate, and then (2) updating/pruning the signal estimate by computing and applying weights, based on the previous signal estimate (wavelet coefficients) and on the BLS-GM model and hierarchical structural dependency modeling. This incorporates structural and statistical dependencies of neighboring coefficients within the sparse transform domain.

The neighborhood is defined as the spatially-adjacent coefficients in the same subband $(v_1, \ldots, v_8)$ (for a 3×3 neighborhood) as well as the parent coefficient (v_p) at the next coarser scale of the wavelet decomposition:

$$\mathbf{v} = [v_1, \ldots, v_8, v_p]^T. \tag{10}$$

The Bayes Least Squares (BLS) estimate of the center coefficient (v_c) can be derived by modeling the local cluster as a Gaussian-scale Mixture:

$$\mathbf{v} \stackrel{d}{=} \sqrt{z}\mathbf{u}, \tag{11}$$

where $\stackrel{d}{=}$ indicates equality in distribution, $\mathbf{u}$ is a zero-mean Gaussian vector and z is an independent positive scalar random variable (known as the *multiplier*), where the density of $\mathbf{v}$ is determined by

$$p_{\mathbf{v}}(\mathbf{v}) = \int p(\mathbf{v} \mid z) p_z(z) \mathrm{d}z. \tag{12}$$

In Gaussian-scale Mixtures the conditional density of $\mathbf{v}$ given z is also Gaussian, therefore the density of $\mathbf{v}$ is an infinite mixture of Gaussians with a mixing density $p_z(z)$. GM densities are symmetric and zero-mean, and they have leptokurtotic marginal densities (i.e., heavier tails than a Gaussian). The scalar z acts as a local variance of a set of

DOI: 10.2352/ISSN.2470-1173.2016.19.COIMG-173

highly correlated coefficients by modulating their values. This enables the GM model to accurately characterize the high-kurtosis nature of the wavelet coefficient marginals in images.[25] Therefore, the BLS-GM model captures local dependencies between neighbors in similar locations, scales, and orientations, and is particularly suited for capturing dependencies in images, here utilized in the sparsity domain.

Noisy observations can be given by

$$\mathbf{y} = \mathbf{v} + \mathbf{e} = \sqrt{z}\mathbf{u} + \mathbf{e}, \tag{13}$$

where $\mathbf{e}$ denotes the noise vector. Given that $\mathbf{u}$ and $\mathbf{e}$ are independent, zero-mean Gaussian vectors with covariance matrices $\mathbf{C_u}$ and $\mathbf{C_e}$, respectively, the random variables $\mathbf{u}$, z, and $\mathbf{e}$ are independent. Under these conditions, an estimate of a coefficient v_c in the center of a particular observed neighborhood $\mathbf{y}$ is given by

$$\hat{v}_c = E\{v_c \mid \mathbf{y}\} = \int p(z \mid \boldsymbol{y}) E\{v_c \mid \mathbf{y}, z\} \mathrm{d}z. \tag{14}$$

This conditional mean given the observation $\mathbf{y}$ can be numerically determined using a local Wiener estimate for $E\{v_c \mid \mathbf{y}, z\}$ and the posterior mixing density $p(z \mid \boldsymbol{y})$.[24] This is utilized in the implementation of the proposed algorithms.

GM-BCS-SPL ALGORITHM IMPLEMENTATION

The proposed Bayes Least Squares-Gaussian-scale Mixtures model Block-based Compressed Sensing Smoothed Projected Landweber (GM-BCS-SPL) adds a Bayes Least Squares (BLS) Gaussian-scale Mixtures (GM) model to account for dependencies between wavelet coefficients in the sparsity domain. The BLS-GM model is imposed to model and account for variances and changing dependencies in highly correlated coefficients in similar locations, scales, and orientations. The GM model is applied to update coefficients before thresholding. Hierarchical structural dependency modeling is incorporated, taking into account parent–child hierarchical coefficient relationships, as well as in-band neighborhood coefficients.

A Gaussian distribution with heavy tails, such as Gaussian-scale Mixtures, tends to characterize the signal data in the transform domain of the DWT, DCT, CT, and DDWT transforms for natural images. This has also been shown to be the case in related research in image denoising in characterizing image data in wavelet transform domains.[24] The transform domains of the DWT, DCT, CT, and DDWT transforms extract different components/frequencies of the signals, and application of the Gaussian-Scale Mixtures model to these similar components/frequencies improves the overall image quality, as shown in Tables II and III and in Figure 2.

The updated algorithmic implementation, modified from the Block Compressed Sensing (BCS)[27] and Block-based Compressed Sensing Smoothed Projected Landweber (BCS-SPL),[13] for the computation of the approximation of the image is as shown in Table I. The algorithm was implemented in Matlab utilizing and building upon the BCS-SPL algorithm available at http://www.ece.msstate.ed

Table I. GM BCS-SPL algorithm implementation.

```
% Inputs:
%   y: CS Measurements
%   Φ_B: Sensing Matrix
%   Ψ: Sparsity Transform
%   λ: Lagrange Multiplier
%   nhood: Transform Coefficient Neighborhood
%
% Outputs:
%   x̂: Estimate of x

% Within Main Program:
%
  read y
  construct Φ_B
  specify Ψ
  input λ
  i = −1
  do
    i = i + 1
    x̂^(i+1) = SPL(x^(i), y, Φ_B, Ψ, λ)
  while(#_of_iterations OR error < error_threshold)
% GM BCS-SPL Algorithm
%
  function x̂^(i+1) = SPL(x^(i), y, Φ_B, Ψ, λ)
    ẋ^(i) = Wiener(x^(i))
    for each block j
      ẍ_j^(i) = ẋ_j^(i) + Φ_B^T(y − Φ_B ẋ_j^(i))
    x̃^(i) = Ψ ẍ^(i)
    σ^(i) = median(|HH1(x̃^(i))|)/0.6745
    x̃_parent^(i) = x̃^(i){scale + 1}{direction};
    x̃_GM^(i) = GM_Model_2D_Structured(x̃^(i), nhood, σ^(i), x̃_parent^(i))
    x̆^(i) = Threshold(x̃_GM^(i), x̃_parent^(i), σ^(i)′ ∗ λ)
    x̄^(i) = Ψ^−1 x̆^(i)
    for each block j
      x̂_j^(i+1) = x̄_j^(i) + Φ_B^T(y − Φ_B x̄_j^(i))
  return x̂^(i+1)
% GM_Model_2D_Structured
%
  function [x̃_GM, σ] = GM_Model_2D_Structured(x̃, nhood, σ, x̃_parent)
    [M N] = size(nhood);
    if (x̃_parent = 0)
      μ_local = filter2(ones(nhood), x̃)/prod(nhood);
      σ_local = filter2(ones(nhood), x̃^2)/prod(nhood) − μ_local^2;
    else
      μ_local = filter2(ones(nhood), x̃)/prod(nhood);
      μ_local = ((μ_local ∗ M ∗ N) + filter2(ones([1 1]), x̃_parent))/(M ∗ N + 1);
      σ_local = (((filter2(ones(nhood), x̃^2)/prod(nhood)) ∗ M ∗ N)+
                (filter2(ones([1 1]), x̃_parent^2)))/(M ∗ N + 1) − μ_local^2;
    end
    if (isempty(σ))
      σ = mean2(σ_local);
    end
    x̃_GM = μ_local + (max(0, σ_local − σ)/max(σ_local, σ)) ∗ (x̃ − μ_local);
  return [x̃_GM, σ]
```

DOI: 10.2352/ISSN.2470-1173.2016.19.COIMG-173

u/~fowler/BCSSPL/, the Contourlet Toolbox (http://www.ifp.illinois.edu/~minhdo/software/), and the Polytechnic Institute Wavelet Software package (http://eeweb.poly.edu/iselesni/WaveletSoftware/).

The noise variance estimate, σ, quantifies the severity of the undersampling artifacts and measurement noise. The sample variance of the noise is proportional to the sample variance of the noisy wavelet coefficients in the highest-frequency subband (here represented as HH1). As such, the sample variance of the noise is estimated using a robust median estimator[28] applied to the highest-frequency subband, as shown in Table I. Since the reconstruction error is reduced throughout the iterations, σ is re-estimated at each iteration. The estimate of σ is used for both the BLS-GM structured modeling and for the Threshold function. Operations within the GM_Model_ 2D_Structured function could be reduced for computational speed (such as cancellation of the multiplication of M * N with division of prod(nhood)), but all operations are shown here for clarity. The GM_Model_2D_Structured function allows for application of Bayes Least Squares-Gaussian-scale Mixtures modeling and hierarchical structural dependency modeling of parent–child coefficient relationships, as well as optimization of the transform coefficient neighborhood size for in-band modeling of Gaussian-scale mixtures.

The Threshold ($\bullet$) operator in SPL is the MAP estimator of the transform coefficient, v, given its parent coefficient, v_p, in the next coarser scale:

$$\text{Threshold}(v,\lambda) = \frac{\left(\sqrt{v^2+v_p^2} - \lambda\sqrt{3\sigma^{(k)}}\Big/\sigma_v\right)_+}{\sqrt{v^2+v_p^2}} v, \quad (15)$$

where $(g)_+ = 0$ for $g < 0$ and $(g)_+ = g$ otherwise. $\sigma^{(k)}$ is the median estimator as described above, σ_v^2 is the marginal variance of coefficient v estimated in a local 3×3 neighborhood surrounding v, as described in Ref. 29, and λ is a convergence-control factor.

As shown in Table I, multiple SPL stages are employed to refine performance. In our experiments, we used ten stages as a near-optimal iteration value based on convergence curve plots for the number of stages versus reconstruction error.

We optimized the in-band neighborhood size within the transform domain for application of the structural and statistical modeling, as well as optimizing the inclusion of the parent coefficient within the structural and statistical modeling.

Different sensing matrices have been used in compressed sensing. Here, we use structurally-random matrices (SRMs)[30,31] used as a sensing matrix in the image/spatial domain. SRMs are based on the scrambled block Hadamard ensemble, and the resulting structured sampling eliminates the need for dense measurement matrices and is thus suitable for large images. SRM-based sensing also has the advantages of low implementation complexity and nearly optimal performance in terms of the required number of measurements for exact recovery.

As in[13] we use the highly-directional transform Dual-tree Discrete Wavelet Transform (DDWT) proposed by Kingsbury in Ref. 32. In the DDWT, real-valued wavelet filters produce the real and imaginary parts of the transform in parallel decomposition trees. DDWT yields a decomposition with a much higher degree of directionality than that possessed by the traditional DWT; however, since both trees of the DDWT are themselves orthonormal or biorthogonal decompositions, the DDWT taken as a whole is a redundant tight frame. The use of a highly-directional transform, and in particular the DDWT, has been shown to provide improved reconstruction performance.[13]

We also employ our algorithmic implementation using the CT transform, which couples a Laplacian-pyramid decomposition with directional filterbanks, inheriting the redundancy of the Laplacian pyramid (i.e., 4/3).[33] Additionally, we employ our algorithmic implementation using the DWT transform for a baseline comparison with other algorithms and using the DCT transform which has demonstrated strong sparsifying properties.

We implement our algorithmic enhancement within the Smoothed Projected Landweber (SPL) structure in order to apply the thresholding and bivariate shrinkage techniques in combination with highly-directional transforms and image-optimized structural and statistical modeling of dependencies.

Finally, we implement a block-based CS (BCS) algorithmic version in order to achieve the superior CPU execution times characteristic of BCS algorithms.

EXPERIMENTAL RESULTS

Existing databases can be utilized for test data and to provide meaningful comparisons with existing algorithms and techniques to quantify performance improvements of feature optimization and overall image quality achieved by addressing variable dependencies in image reconstruction. For comparison purposes, standard images used in recent publications for testing of compressed sensing algorithms were used, including the images commonly known as 'Lenna' and 'Barbara' (widely used in image processing literature) and images from several classes of the Microsoft Research Image Database available at http://research.microsoft.com/en-us/projects/. Images from classes were chosen based on the greatest appearance of randomness—as being the images of most interest to target for high-performance compressed sensing algorithms. As shown in Figure 1, eight images were selected: "Lenna" and "Barbara" (from the University of Southern California (USC) Signal and Image Processing Institute (SIPI) Image Database), and Flowers_109_0983, Birds_111_1163, Sheep_117_1760, Buildings_152_5234, Countryside_152_5249, and Urban_184_8487 representing six classes of images from the Microsoft Research Image Database.

Experiments were carried out on 512×512 gray-scale images. Since the quality of reconstruction can vary due to the randomness of the measurement matrix, $\mathbf{\Phi}_B$, reconstruction error and Peak Signal-to-Noise Ratio (PSNR) are averaged over five independent trials. Also, five different

DOI: 10.2352/ISSN.2470-1173.2016.19.COIMG-173

Figure 1. Original 512 × 512 Images: (a) ''Lenna'' and (b) ''Barbara'' from the USC-SIPI Image Database, and (c) Flowers_109_0983, (d) Birds_111_1163, 1 (e) Sheep_117_1760, (f) Buildings_152_5234, (g) Countryside_152_5249, and (h) Urban_159_5923 from the Microsoft Research Image Database.

Figure 2. Reconstructed ''Lenna'' image at the lowest subrate of 0.1 (highest CS ratio) for the original algorithms: (a) BCS-SPL-DWT, (b) BCS-SPL-DCT, (c) BCS-SPL-CT, and (d) BCS-SPL-DDWT, and for the enhanced algorithms: (e) GM-BCS-SPL-DWT, (f) GM-BCS-SPL-DCT, (g) GM-BCS-SPL-CT, and (h) GM-BCS-SPL-DDWT.

subrates were used corresponding to measurement ratios (M/N) of 0.1, 0.2, 0.3, 0.4, and 0.5, respectively. For the bivariate shrinkage we used $\lambda = 20$ for BCS-SPL-DWT and GM-BCS-SPL-DWT, $\lambda = 25$ for BCS-SPL-DDWT and GM-BCS-SPL-DDWT, $\lambda = 6$ for BCS-SPL-DCT and GM-BCS-SPL-DCT, and $\lambda = 10$ for BCS-SPL-CT and

DOI: 10.2352/ISSN.2470-1173.2016.19.COIMG-173

Table II. Relative l_2 norm of reconstruction error.

Image Lenna						Image Sheep					
	CS ratio						CS ratio				
Algorithm	0.1	0.2	0.3	0.4	0.5	Algorithm	0.1	0.2	0.3	0.4	0.5
GM-BCS-SPL-DDWT	**0.055514**	**0.039771**	**0.031687**	**0.026287**	**0.022146**	GM-BCS-SPL-DDWT	0.060628	0.048533	0.040574	0.033437	0.027799
GM-BCS-SPL-CT	0.057366	0.041702	0.033581	0.027938	0.023551	GM-BCS-SPL-CT	0.057390	0.043427	0.036247	0.030730	0.026167
GM-BCS-SPL-DCT	0.058251	0.042708	0.034068	0.028202	0.023556	GM-BCS-SPL-DCT	**0.055022**	**0.041726**	**0.034736**	**0.029356**	**0.024481**
GM-BCS-SPL-DWT	0.058505	0.041798	0.033446	0.027821	0.023470	GM-BCS-SPL-DWT	0.058125	0.044092	0.036372	0.030545	0.025745
BCS-SPL-DDWT	0.056602	0.039836	**0.031685**	**0.026285**	**0.022144**	BCS-SPL-DDWT	0.060663	0.048555	0.040577	0.033459	0.027814
BCS-SPL-CT	0.057504	0.041717	0.033557	0.027912	0.023519	BCS-SPL-CT	0.058057	0.043344	0.036169	0.030654	0.026103
BCS-SPL-DCT	0.059995	0.043970	0.035390	0.029414	0.024767	BCS-SPL-DCT	0.059797	0.046903	0.039431	0.033560	0.028429
BCS-SPL-DWT	0.058888	0.041946	0.033455	0.027807	0.023453	BCS-SPL-DWT	0.058575	0.044050	0.036331	0.030513	0.025712
Image Barbara						Image Buildings					
GM-BCS-SPL-DDWT	**0.112080**	0.094850	0.080273	0.067426	0.056241	GM-BCS-SPL-DDWT	0.097451	0.078910	**0.066705**	**0.056924**	**0.048640**
GM-BCS-SPL-CT	0.113630	0.094076	**0.078492**	**0.064723**	**0.052915**	GM-BCS-SPL-CT	**0.096053**	**0.078224**	0.066921	0.057899	0.049907
GM-BCS-SPL-DCT	0.112650	**0.093819**	0.078545	0.065917	0.055046	GM-BCS-SPL-DCT	0.096458	0.080613	0.070126	0.060817	0.052231
GM-BCS-SPL-DWT	0.115360	0.098536	0.084610	0.072122	0.060610	GM-BCS-SPL-DWT	0.099682	0.080766	0.068134	0.058224	0.049625
BCS-SPL-DDWT	0.113340	0.095332	0.080264	0.067413	0.056207	BCS-SPL-DDWT	0.098564	0.079478	0.066795	0.056931	0.048645
BCS-SPL-CT	0.113820	0.094330	0.078628	0.064833	0.052988	BCS-SPL-CT	0.096424	0.078305	0.066955	0.057862	0.049875
BCS-SPL-DCT	0.114240	0.094222	0.078496	0.065980	0.053967	BCS-SPL-DCT	0.100140	0.082471	0.077345	0.063457	0.055099
BCS-SPL-DWT	0.115680	0.099003	0.085082	0.072315	0.060681	BCS-SPL-DWT	0.100300	0.081229	0.068325	0.058256	0.049636
Image Flowers						Image Countryside					
GM-BCS-SPL-DDWT	**0.081818**	0.050758	**0.036308**	**0.027148**	**0.020995**	GM-BCS-SPL-DDWT	0.060958	0.049035	**0.041698**	**0.035923**	**0.030729**
GM-BCS-SPL-CT	0.081925	0.051591	0.037865	0.029073	0.023014	GM-BCS-SPL-CT	0.059233	**0.048490**	0.042095	0.036793	0.031884
GM-BCS-SPL-DCT	0.082146	0.051102	0.037006	0.028221	0.022191	GM-BCS-SPL-DCT	**0.058787**	0.049041	0.042857	0.037599	0.032466
GM-BCS-SPL-DWT	0.083919	0.051087	0.036760	0.027746	0.021675	GM-BCS-SPL-DWT	0.060387	0.049372	0.042410	0.036731	0.031446
BCS-SPL-DDWT	0.081866	**0.050748**	0.036336	0.027161	0.021008	BCS-SPL-DDWT	0.061196	0.049089	0.041714	0.035935	**0.030728**
BCS-SPL-CT	0.082719	0.051727	0.037920	0.029125	0.023047	BCS-SPL-CT	0.059271	0.048504	0.042104	0.036801	0.031888
BCS-SPL-DCT	0.086663	0.053932	0.039307	0.029992	0.023582	BCS-SPL-DCT	0.060080	0.050157	0.043832	0.038427	0.033272
BCS-SPL-DWT	0.085620	0.051299	0.036822	0.027782	0.021703	BCS-SPL-DWT	0.060870	0.049561	0.042526	0.036782	0.031471
Image Birds						Image Urban					
GM-BCS-SPL-DDWT	0.080060	0.062991	0.051392	0.041647	0.033702	GM-BCS-SPL-DDWT	0.074150	0.054153	**0.041197**	**0.033052**	**0.027105**
GM-BCS-SPL-CT	0.076394	0.058106	0.047097	0.038713	0.031998	GM-BCS-SPL-CT	**0.072760**	**0.052461**	0.041652	0.034078	0.028242
GM-BCS-SPL-DCT	**0.074823**	**0.056394**	**0.045286**	**0.036834**	**0.030124**	GM-BCS-SPL-DCT	0.072839	0.053726	0.043017	0.035300	0.029221
GM-BCS-SPL-DWT	0.079496	0.061931	0.050311	0.041375	0.034357	GM-BCS-SPL-DWT	0.074370	0.052631	0.041327	0.033492	0.027519
BCS-SPL-DDWT	0.080067	0.062992	0.051406	0.041659	0.033712	BCS-SPL-DDWT	0.074195	0.054160	0.041207	0.033057	0.027109
BCS-SPL-CT	0.076270	0.057961	0.046972	0.038616	0.031920	BCS-SPL-CT	0.072887	0.052524	0.041713	0.034133	0.028291
BCS-SPL-DCT	0.081458	0.062683	0.050990	0.042142	0.034906	BCS-SPL-DCT	0.073965	0.054548	0.043694	0.035900	0.029903
BCS-SPL-DWT	0.079514	0.061845	0.050244	0.041326	0.034316	BCS-SPL-DWT	0.074992	0.052921	0.041403	0.033519	0.027534

GM-BCS-SPL-CT. Finally, up to 200 iterations of each algorithm were performed to allow for convergence of each algorithm.

Reconstruction accuracy was evaluated as the relative l_2 norm of reconstruction error, defined by

$$\|\mathbf{y} - \hat{\mathbf{y}}\|_2 / \|\mathbf{y}\|_2, \tag{16}$$

where $\mathbf{y}$ is the original signal and $\hat{\mathbf{y}}$ is the recovered image. In Table II, results are shown for the l_2 norm reconstruction error for the eight algorithms: GM-BCS-SPL-DDWT, GM-BCS-SPL-CT, GM-BCS-SPL-DCT, GM-BCS-SPL-DWT, BCS-SPL-DDWT, BCS-SPL-CT, BCS-SPL-DCT, and BCS-SPL-DWT. Corresponding reconstruction error is lower for the proposed algorithms, particularly at the lower sampling rates of interest in compressed sensing. Due to the random and highly varying nature of image data, occasionally the GM-algorithmic version of a particular transform does not result in improvement and

DOI: 10.2352/ISSN.2470-1173.2016.19.COIMG-173

Table III. PSNR performance in dB.

Image Lenna						Image Sheep					
	CS ratio						CS ratio				
Algorithm	0.1	0.2	0.3	0.4	0.5	Algorithm	0.1	0.2	0.3	0.4	0.5
GM-BCS-SPL-DDWT	**28.2989**	**31.3734**	33.4567	35.1782	36.7481	GM-BCS-SPL-DDWT	30.3842	32.4603	34.0337	35.6702	37.2388
GM-BCS-SPL-CT	28.1015	30.9747	32.9425	34.6332	36.1956	GM-BCS-SPL-CT	30.5930	33.1003	34.7192	36.1829	37.6132
GM-BCS-SPL-DCT	27.9572	30.7693	32.8242	34.5624	36.2128	GM-BCS-SPL-DCT	**30.8980**	**33.4287**	**35.0926**	**36.5994**	**38.1985**
GM-BCS-SPL-DWT	27.7444	30.8775	32.9361	34.6384	36.2071	GM-BCS-SPL-DWT	30.4810	33.0015	34.7201	36.2640	37.7790
BCS-SPL-DDWT	28.0797	31.3550	**33.4578**	**35.1791**	**36.7489**	BCS-SPL-DDWT	30.3757	32.4569	34.0335	35.6655	37.2348
BCS-SPL-CT	28.0801	30.9709	32.9488	34.6417	36.2081	BCS-SPL-CT	30.4497	33.1170	34.7385	36.2064	37.6355
BCS-SPL-DCT	27.6713	30.4916	32.4873	34.1982	35.7832	BCS-SPL-DCT	30.1614	32.4328	34.0190	35.4698	36.9580
BCS-SPL-DWT	27.6680	30.8368	32.9326	34.6425	36.2137	BCS-SPL-DWT	30.3869	33.0080	34.7301	36.2730	37.7902
Image Barbara						Image Buildings					
GM-BCS-SPL-DDWT	22.7421	24.1957	25.6750	27.1988	28.7963	GM-BCS-SPL-DDWT	24.4239	26.2946	**27.7920**	**29.2035**	**30.5930**
GM-BCS-SPL-CT	22.7293	24.3007	25.8654	**27.5532**	**29.3247**	GM-BCS-SPL-CT	**24.6496**	**26.4039**	27.7724	29.0494	30.3573
GM-BCS-SPL-DCT	**22.8406**	**24.3835**	**25.9178**	27.3907	28.9344	GM-BCS-SPL-DCT	24.5997	26.1749	27.4255	28.6831	30.0172
GM-BCS-SPL-DWT	22.4345	23.8297	25.1633	26.5358	28.0417	GM-BCS-SPL-DWT	24.1572	26.0743	27.5930	28.9928	30.4053
BCS-SPL-DDWT	22.5769	24.1392	25.6746	27.1999	28.8022	BCS-SPL-DDWT	24.2910	26.2245	27.7781	29.2020	30.5919
BCS-SPL-CT	22.7067	24.2696	25.8440	27.5328	29.3066	BCS-SPL-CT	24.6133	26.3945	27.7688	29.0536	30.3627
BCS-SPL-DCT	22.7507	24.3599	25.9172	27.3991	29.1679	BCS-SPL-DCT	24.2942	25.9860	26.6386	28.3465	29.5902
BCS-SPL-DWT	22.3936	23.7733	25.0995	26.5052	28.0263	BCS-SPL-DWT	24.0733	26.0121	27.5643	28.9865	30.4013
Image Flowers						Image Countryside					
GM-BCS-SPL-DDWT	**29.5977**	33.7338	**36.6126**	**39.1216**	**41.3571**	GM-BCS-SPL-DDWT	27.7174	29.5305	**30.9541**	**32.2853**	**33.6643**
GM-BCS-SPL-CT	29.5621	33.4149	36.0785	38.3970	40.4622	GM-BCS-SPL-CT	27.9343	**29.6291**	30.8767	32.0707	33.3372
GM-BCS-SPL-DCT	29.5017	33.5457	36.3525	38.7302	40.8491	GM-BCS-SPL-DCT	**27.9461**	29.5071	30.6907	31.8910	33.1805
GM-BCS-SPL-DWT	29.2224	**33.4728**	36.3188	38.7913	40.9712	GM-BCS-SPL-DWT	27.6343	29.4040	30.7830	32.0777	33.4524
BCS-SPL-DDWT	29.5896	**33.7351**	36.6075	39.1186	41.3517	BCS-SPL-DDWT	27.6308	29.5044	30.9470	32.2813	**33.6646**
BCS-SPL-CT	29.4656	33.3885	36.0582	38.3712	40.4382	BCS-SPL-CT	27.9263	29.6237	30.8728	32.0678	33.3355
BCS-SPL-DCT	29.0473	33.0470	35.8065	38.2012	40.3229	BCS-SPL-DCT	27.7664	29.3253	30.5189	31.6956	32.9640
BCS-SPL-DWT	28.9989	33.4185	36.2894	38.7633	40.9421	BCS-SPL-DWT	27.5277	29.3576	30.7516	32.0619	33.4436
Image Birds						Image Urban					
GM-BCS-SPL-DDWT	28.4463	30.6033	32.4031	34.2124	36.0343	GM-BCS-SPL-DDWT	23.2439	25.9402	**28.2326**	**30.1381**	**31.8851**
GM-BCS-SPL-CT	28.7556	31.1432	33.0039	34.7306	36.4111	GM-BCS-SPL-CT	**23.3328**	**26.0737**	28.0802	29.8304	31.4812
GM-BCS-SPL-DCT	**28.8926**	**31.3931**	**33.3464**	**35.1758**	**36.9532**	GM-BCS-SPL-DCT	23.2083	25.8276	27.7759	29.5145	31.1791
GM-BCS-SPL-DWT	28.4236	30.6303	32.4615	34.1759	35.8087	GM-BCS-SPL-DWT	22.8972	25.9454	28.0928	29.9455	31.6779
BCS-SPL-DDWT	28.4459	30.6034	32.4008	34.2103	36.0319	BCS-SPL-DDWT	23.2214	25.9391	28.2310	30.1370	31.8839
BCS-SPL-CT	28.7693	31.1657	33.0280	34.7529	36.4326	BCS-SPL-CT	23.3189	26.0644	28.0676	29.8177	31.4675
BCS-SPL-DCT	28.1579	30.4775	32.3243	34.0224	35.6920	BCS-SPL-DCT	23.0854	25.6903	27.6192	29.3646	30.9694
BCS-SPL-DWT	28.4141	30.6424	32.4732	34.1864	35.8194	BCS-SPL-DWT	22.8032	25.8868	28.0741	29.9374	31.6724

may result in a slight degradation; however, one of the GM-algorithmic versions always has the best performance over all other algorithms at the lowest sampling rates. Reconstruction accuracy is closer between several algorithms at the higher sampling rates, which is not surprising since the higher sampling rates (sampled in the transform domain) contain a greater percentage of the image data. The GM-algorithmic versions provide improved performance, and the improved minimization of reconstruction error is statistically significant. It is noted that the proposed algorithmic modification demonstrates enhanced performance refinement improvements over state-of-the-art CS image reconstruction algorithms that already achieve exceptional performance.

Performance results were also compared based on the computed PSNR in dB for the reconstructed images for the original and proposed algorithms. Table III shows the PSNR for the eight algorithms: GM-BCS-SPL-

DOI: 10.2352/ISSN.2470-1173.2016.19.COIMG-173

DDWT, GM-BCS-SPL-CT, GM-BCS-SPL-DCT, GM-BCS-SPL-DWT, BCS-SPL-DDWT, BCS-SPL-CT, BCS-SPL-DCT, and BCS-SPL-DWT.

As with the l_2 norm reconstruction error results, the corresponding PSNRs of the proposed GM-algorithmic versions outperform the original algorithms, particularly at the lowest sampling rates (highest CS ratios), with performance much closer at the higher sampling rates. As can be seen, the GM-BCS-SPL-DDWT algorithm has the best performance for the 'Lenna' image at the highest compressed sensing ratios, with performance very close between the GM-BCS-SPL-DDWT and BCS-SPL-DDWT algorithms at the higher sampling rates that contain more of the information. For the 'Barbara' image, the GM-BCS-SPL-DDWT and GM-BCS-SPL-DCT algorithms outperform all other algorithms at the lowest sampling rates, while the GM-BCS-SPL-CT algorithm has the best performance at the higher sampling rates. For the 'flowers', image, the GM-BCS-SPL-DDWT algorithm outperforms all other algorithms at each sampling rate except for the 0.2 subrate where the BCS-SPL-DDWT had slightly better performance. For the 'Birds' and 'Sheep' images, the GM-BCS-SPL-DCT algorithm outperforms all other algorithms. For the 'Buildings', 'Countryside', and 'Urban' images, the GM-BCS-SPL-CT algorithm, and GM-BCS-SPL-DCT for the 'Countryside' image, outperform all other algorithms at the highest CS ratios, while the GM-BCS-SPL-DDWT provides better performance at the highest sampling rates.

As expected, performance results are similar in terms of the PSNR as to the relative l_2-norm of reconstruction error, with the proposed GM modification providing improved results at the lower measurement rates. The improvement in performance is statistically significant at the lowest sampling rates. At higher sampling rates the performance is close for all algorithms with statistically close results between the GM and non-GM algorithmic versions. Of course, the higher sampling rates contain a higher percentage of the signal information. In CS, the goal is optimal reconstruction given highly compressed sensing of signals (low sampling rates). The proposed algorithms show performance improvements over current state-of-the-art CS image reconstruction algorithms.

Fig. 2 shows the reconstructed 'Lenna' image for the lowest subrate of 0.1 (highest CS ratio) for the original algorithms and enhanced algorithms. Comparing the images of the block-based SPL-DWT, -DCT, -CT, and -DDWT algorithms with the modified block-based GM-SPL-DWT, -DCT, -CT, and -DDWT algorithms, it can be seen that the overall image quality shows improvement. There are still some artifacts present due to the block-based implementation. These artifacts are not present if computations are performed over the entire signal. Therefore, a trade-off exists, as usual, with regard to computational time/efficiency versus image quality with regard to these artifacts. However, the modified algorithm shows overall improvement in image quality and can be implemented across the entire signal for very-high-quality image reconstruction with compressed sampling or implemented in the efficient block-based implementation for higher-quality images with efficient and reduced computational processing.

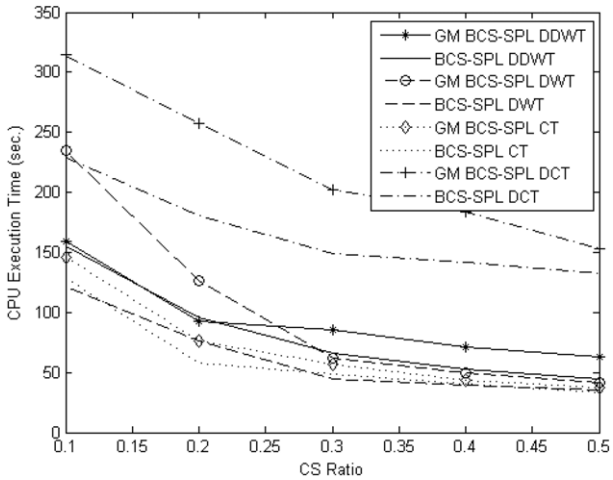

Figure 3. Reconstruction time for the "Lenna" image.

Comparing the BCS-SPL-DDWT and the GM-BCS-SPL-DWT with the GM-BCS-SPL-DDWT, it can be seen that neither the application of highly-directional and redundant transforms nor the application of the GM structural and statistical dependency modeling in the sparsity domain alone provides the performance achieved as to when the GM and hierarchical structural dependency modeling is combined with highly-directional and redundant transforms. Optimized performance is achieved when the GM and hierarchical structural dependency modeling is applied in the sparsity domain of highly-directional and redundant transforms. Within the GM-BCS-SPL-DDWT, the GM and hierarchical structural dependency modeling provides optimized values as input to the bivariate shrinkage algorithm in the transform domain.

The proposed GM-BCS-SPL algorithms always statistically match or outperform the original BCS-SPL algorithms at the lowest sampling rates, even outperforming the smoothed and highly-directional BCS-SPL-DDWT.

The reconstruction time for the 'Lenna' image for each algorithm and CS ratio is shown in Figure 3. CPU reconstruction time is shown for algorithm execution on a 1.6 GHz AMD E-350 dual-core processor. Due to the added complexity of imposing the BLS-GM model, the total computation time of the proposed algorithms is slightly longer than the original algorithms. The CPU execution times of the proposed GM-algorithmic versions are very close to the fast CPU computation times of the original algorithms. In addition, the GM-algorithmic versions converge in approximately 20 iterations on average, resulting in fast execution times for the additional algorithmic complexity. In fact, the reconstruction time of the GM-BCS-SPL-DDWT algorithm is actually faster than that of the BCS-SPL-DDWT at the lowest subrate for the "Lenna" image due to the faster convergence of the GM-algorithmic version.

It can be seen that the computation time of each GM algorithm is still consistent with the superior computational times provided by block-based compressed sensing, which

DOI: 10.2352/ISSN.2470-1173.2016.19.COIMG-173

tends to be an order of magnitude faster than non-block-based algorithms, as noted above. In addition, block-based compressed sensing algorithms have the added advantage of increased throughput in implementation because computations can be performed on a block-by-block basis, so that the encoder does not need to wait until the entire image is processed, but may send each block after its linear projection.

SUMMARY

Highly-directional and redundant transforms, thresholding and shrinkage techniques, and structural and statistical modeling of images were employed to yield improved reconstruction performance of images in compressed sensing. Exploitation of hierarchical structure and multiscale subbands of frequency and orientation provides increased selectivity across orientations, scales, and frequencies. In addition, the application of Bayes Least Squares (BLS)-Gaussian-scale Mixtures (GM) modeling, shown to accurately model the statistics of natural images (including local clustering and leptokurtotic marginal statistics), was incorporated through weights in the reconstruction algorithm. Hierarchical structural dependency modeling was incorporated by taking into account parent–child coefficient dependencies in the transform domain. This modeling of structural and statistical dependencies applied with the selectivity of highly-directional transforms across orientations, scales, and frequencies provided improved performance over current state-of-the-art algorithms. The new algorithmic versions were implemented in block-based CS (BCS) algorithms and are denoted as GM-BCS-SPL-DWT, GM-BCS-SPL-DCT, GM-BCS-SPL-CT, and GM-BCS-SPL-DDWT.

Various classes of images were tested, including people, nature, animals, buildings, and urban and countryside scenes. For each of these classes of images, a GM-algorithmic version obtained superior image reconstruction performance. In all classes of images tested, a GM-algorithmic version provided the most superior image reconstruction accuracy, particularly at the most compressed sampling rates of greatest interest in compressed sensing.

The GM algorithms particularly offer improved performance for natural images, and natural images tend to have non-linear mixtures incorporating more highly-random-appearing dependencies. The GM algorithms provide the algorithmic robustness needed to address these dependencies, which tend to be more difficult to account for, particularly in compressed sensing.

POTENTIAL FUTURE DIRECTIONS

Structural dependency models could be designed for specific signal characteristics for specific classes/characteristics of images. Potential performance enhancements could be obtained by combining this method with automating identification of repetitive patterns and structural details, using additional sharpening operations to identify edge components, and reducing residual aliasing artifacts/reconstruction artifacts. This could be incorporated within the framework of compressed/sparse sensing to provide performance improvements. Combining this with optimization of the basis set formation/feature extraction for non-linearly mixed signals could provide further optimization.

Unsupervised learning and iteration could be used to develop predictions and to test for measurement consistency. Unsupervised learning provides automatic clustering of features. It gives insight about the existent structures and patterns in data. It enables more adaptive and meaningful classes corresponding to the natural characteristics of the data.

REFERENCES

[1] D. L. Donoho, "Compressed sensing," IEEE Trans. Inf. Theory **52**, 1289–1306 (2006).

[2] E. J. Candès, J. Romberg, and T. Tao, "Robust uncertainty principles: exact signal reconstruction from highly incomplete frequency information," IEEE Trans. Inf. Theory **52**, 489–509 (2006).

[3] L. M. Keuthan, R. J. Harrington, and J. M. Willey, "Image reconstruction in the presence of non-linear mixtures utilizing wavelet variable-dependency modeling in compressed sensing algorithms," Proc. SPIE **9401**, 1–14 (2015).

[4] E. J. Candès, "Compressive sampling," *Proc. Int. Congr. Math.* (2006), pp. 1433–1452.

[5] E. J. Candès, J. Romberg, and T. Tao, "Stable signal recovery from incomplete and inaccurate measurements," Commun. Pure Appl. Math. **59**, 1207–1223 (2006).

[6] M. Davenport, M. Duarte, C. Hegde, and R. Baraniuk, *Introduction to Compressive Sensing*, Ch. 3., Retrieved from the OpenStax-CNX Web site: http://cnx.org/content/m37172/1.7/ (2011).

[7] R. Garg and R. Khandekar, "Gradient descent with sparsification: an iterative algorithm for sparse recovery with restricted isometry property," *Proc. Annual Int. Conf. Mach. Learn.* (2009), pp. 337–344.

[8] T. Blumensath and M. E. Davies, "Iterative thresholding for sparse approximations," J. Fourier Anal. Appl. **14**, 629–654 (2008).

[9] J. Haupt and R. Nowak, "Signal reconstruction from noisy random projections," IEEE Trans. Inf. Theory **52**, 4036–4048 (2006).

[10] Y. M. Lu and M. N. Do, "Sampling signals from a union of subspaces," IEEE Signal Process. Mag. **25**, 41–47 (2008).

[11] T. Blumensath and M. E. Davies, "Sampling theorems for signals from the union of finite-dimensional linear subspaces," IEEE Trans. Inf. Theory **55**, 1872–1882 (2009).

[12] R. G. Baraniuk, V. Cevher, M. Duarte, and C. Hegde, "Model-based compressive sensing," IEEE Trans. Inf. Theory **56**, 1982–2001 (2010).

[13] S. Mun and J. E. Fowler, "Block compressed sensing of images using directional transforms," *Proc. IEEE Int'l. Conf. on Image Processing (ICIP)* (IEEE, Piscataway, NJ, 2009), pp. 3021–3024.

[14] S. G. Chang, B. Yu, and M. Vetterli, "Spatially adaptive wavelet thresholding with context modeling for image denoising," IEEE Trans. Image Process. **9**, 1522–1531 (2000).

[15] E. P. Simoncelli, "Bayesian denoising of visual images in the wavelet domain," *Bayesian Inference in Wavelet Based Models*, edited by P. Muller and B. Vidakovic (Springer, New York, 1999), Vol. 141, pp. 291–308, ch. 18.

[16] J. Starck, E. J. Candès, and D. L. Donoho, "The curvelet transform for image denoising," IEEE Trans. Image Process. **11**, 670–684 (2002).

[17] V. Strela, J. Portilla, and E. Simoncelli, "Image denoising using a local Gaussian scale mixture model in the transform domain," Proc. SPIE **4119**, 363–371 (2000).

[18] E. P. Simoncelli, W. T. Freeman, E. H. Adelson, and D. J. Heeger, "Shiftable multi-scale transforms," IEEE Trans. Inf. Theory **38**, 587–607 (1992).

[19] E. P. Simoncelli, "Statistical models for images: compression, restoration and synthesis," *Proc. 31st Asilomar Conf. on Signals, Systems and Computers*. [Online], Available: http://www.cns.nyu.edu/~eero/publications.html.

[20] M. K. Mihcak, I. Kozintsev, K. Ramchandran, and P. Moulin, "Low-complexity image denoising based on statistical modeling of wavelet coefficients," IEEE Trans. Signal Process. **6**, 300–303 (1999).

DOI: 10.2352/ISSN.2470-1173.2016.19.COIMG-173

[21] M. Malfait and D. Roose, "Wavelet-based image denoising using a Markov random field a priori model," IEEE Trans. Image Process. **6**, 549–565 (1997).
[22] S. G. Chang, B. Yu, and M. Vetterli, "Spatially adaptive wavelet thresholding with context modeling for image denoising," *Proc. 5th IEEE Int'l. Conf. on Image Processing (ICIP)* (IEEE, Piscataway, NJ, 1998), pp. 535–539.
[23] F. Abramovich, T. Besbeas, and T. Sapatinas, "Empirical Bayes approach to block wavelet function estimation," Comput. Stat. Data Anal. **39**, 435–451 (2002).
[24] J. Portilla, V. Strela, M. J. Wainwright, and E. Simoncelli, "Image denoising using scale mixtures of Gaussians in the wavelet domain," IEEE Trans. Image Process. **12**, 1338–1351 (2003).
[25] M. J. Wainwright and E. P. Simoncelli, "Scale mixtures of Gaussians and the statistics of natural images," Adv. Neural Inf. Process. Syst. **12**, 855–861 (2000).
[26] M. J. Wainwright, E. P. Simoncelli, and A. S. Willsky, "Random cascades on wavelet trees and their use in modeling and analyzing natural imagery," Appl. Comput. Harmon. Anal. **11**, 89–123 (2001).
[27] L. Gan, "Block compressed sensing of natural images," *Proc. Int. Conf. on Digital Signal Processing, Cardiff, UK* (2007), pp. 403–406.
[28] D. L. Donoho, "De-noising by soft-thresholding," IEEE Trans. Inf. Theory **41**, 613–627 (1995).
[29] L. Sendur and I. W. Selesnick, "Bivariate shrinkage functions for wavelet-based denoising exploiting interscale dependency," IEEE Trans. Signal Process. **50**, 2744–2756 (2002).
[30] L. Gan, T. T. Do, and T. D. Tran, "Fast compressive imaging using scrambled block Hadamard ensemble," *Proc. Eur. Signal Processing Conf. (EUSIPCO), Lausanne, Switzerland* (2008), pp. 1–5.
[31] T. T. Do, L. Gan, N. H. Nguyen, and T. D. Tran, "Fast and efficient compressive sensing using structurally random matrices," IEEE Trans. Signal Process. **60**, 139–154 (2012).
[32] N. G. Kingsbury, "Complex wavelets for shift-invariant analysis and filtering of signals," Appl. Comput. Harmon. Anal. **10**, 234–253 (2001).
[33] M. N. Do and M. Vetterli, "The contourlet transform: an efficient directional multiresolution image representation," IEEE Trans. Image Process. **14**, 2091–2106 (2005).